RSC Advances

PAPER

View Article Online
View Journal | View Issue

Cite this: *RSC Adv.*, 2017, **7**, 21918

The influence of epitaxial crystallization on the mechanical properties of a high density polyethylene/reduced graphene oxide nanocomposite injection bar

Guibin Yao,[a] Tianchen Duan,[a] Minfang An,[a] Haojun Xu,[a] Feng Tian[bc] and Zongbao Wang *[a]

Received 6th March 2017
Accepted 13th April 2017

DOI: 10.1039/c7ra02742g

rsc.li/rsc-advances

High density polyethylene (HDPE)/reduced graphene oxide (RGO) nanocomposite bars were prepared by injection molding and the effects of RGO on the HDPE matrix were investigated. Differential scanning calorimetry results demonstrated that RGO was an effective nucleation agent for HDPE. Two dimensional wide angle X-ray diffraction (2D WAXD) results showed that the incorporation of RGO enhanced the degree of orientation of HDPE crystals in the flow direction but had no influence on the crystal structure of HDPE. Two dimensional small angle X-ray scattering (2D SAXS) results confirmed that the orientation of HDPE chains in the flow direction was enhanced with the increase of RGO content, which was attributed to the fact that RGO obstructed the motion of polymer chains. These results indicated that the incorporation of RGO can enhance the crystallization and orientation of the HDPE matrix, resulting in the improvement of mechanical properties.

1. Introduction

Due to its excellent characteristics such as good physical and mechanical properties, chemical resistivity, gas barrier property, easy processing, and its low cost, HDPE has been widely used for film products, plastic products, hollow products, pipe products, fiber products, cable products *etc.*[1–3] However, further extension of the applications of HDPE has been limited by its mechanical properties.[4–6] Therefore, improving the mechanical properties of HDPE is an issue to be solved urgently.[5,6]

Nanocomposite materials in the past decades have attracted scientists' great attention as a promising novel class of materials, which can enhance properties significantly at very low loadings owing to their unique properties and numerous potential applications with greatly increased specific interfacial area.[7–11] It is well known that carbon based fillers, such as diamond and graphite, can particularly enhance the crystallization, orientation and mechanical properties of semi-crystalline polymer.[12] Drzal group showed that nanoparticle was a potential nano-reinforcement and it, as a 0 dimensional (0 D) point, could interact with the polymer matrix in improving the mechanical properties.[13–15] Carbon nano tube (CNT), as 1 dimensional (1 D) material of graphite family, has also been proved that it could spectacularly reinforce the mechanical properties of HDPE matrix.[16–18] However, using carbon nanotubes in nanocomposite still contains many unresolved issues such as low interfacial interactions with the polymeric matrix.[19]

Graphene as the first 2D counterpart of graphite with single sheet was widely used.[20–24] It can also work as filler.[25] It is also found to be the strongest material up to now.[26] A lot of studies showed that graphene could improve the mechanical properties of polymers.[27–29] It is well known that the mechanical properties of polymer/nanofiller composites strongly depend on the interaction between polymer and nanofiller. Great efforts have been devoted to improve the interaction between graphene and polymer matrix.[30–32] However, most researches still use the common methods of other polymer/inorganic nanocomposites to improve the interface adhesion,[33] seldom make the best use of the structure character of graphene and its matching relationship with polymer structure. The researches using nondestructive physical modification methods to increase the interface adhesion between polymer and graphene are less, and the studies about interfacial crystallization to enhanced interaction of polymer/graphene nancomposites are much less. Petermann *et al.* reported that epitaxial interfaces with strong adherence were responsible for the improvement of the mechanical properties of semicrystalline polymers.[34–36] Fukumaru[52] reported that effective interfacial interaction between the polybenzoxazole and CNT could improve the mechanical

[a]*Ningbo Key Laboratory of Specialty Polymers, Faculty of Materials Science and Chemical Engineering, Ningbo University, Ningbo 315211, PR China. E-mail: wangzongbao@nbu.edu.cn*

[b]*Shanghai Institute of Applied Physics, Chinese Academy of Sciences, Shanghai 201204, PR China*

[c]*State Key Laboratory of Polymer Materials Engineering, Sichuan University, Chengdu 610065, PR China*

properties of polymer matrix.[37] In our previous work, the yield strength and Young's modulus of poly(e-caprolactone) (PCL)/RGO nancomposites with epitaxial interaction were improved compared with pure PCL.[38,39]

It is well known that epitaxial crystallization of polymers onto various polymeric substrates, since the early 1980s, has been an extremely active subject in the field of polymer science.[40–42] It is generally accepted that the occurrence of polymer epitaxy is based on some certain crystallographic matches, *e.g.*, a coincidence of unit cell dimensions, and the highest limit for the occurrence of the epitaxial growth is assumed to be 15%.[43] Previous literature showed that polyethylene could epitaxial crystallized on graphene surface, and the mismatch rate was −5.0%.[44] Moreover the melting point of HDPE is much higher than that of PCL, which may resulting in different enhancement of mechanical properties. Therefore HDPE was chosen as a model polymer to study the epitaxial crystallization on RGO.

In this work, we take advantage of the polymer epitaxial crystallization on RGO to improve the interfacial interaction between RGO and HDPE, and study the influence of epitaxial crystallization on the mechanical properties of polymer matrix. The WAXD and SAXS measurements were used to investigate the reinforcement effect and structural mechanism.

2. Experimental

2.1. Materials

HDPE was purchased from Dow Chemical Company, with average weight M_n = 15 820 g mol^{-1} and polydispersity index M_w/M_n = 4.9. Natural flake graphite was purchased from Qingdao Jiuyi graphite Co., Ltd. (Shandong, China) with mean particle size of 50 μm. Hydrochloric acid (HCl) (37%), sulfuric acid (H_2SO_4) (98%), potassium nitrate (KNO_3), potassium permanganate ($KMnO_4$), hydrogen peroxide (H_2O_2) (35%), *n*-hexanol and chloroform were purchased from Sinopharm Chemical Reagent Co., Ltd. (Shanghai, China). All reagents were used as received without further purification.

2.2. Sample preparation

GO was exfoliated by ultra-sonication from graphite oxide which was produced by modified Hummers' method.[45] RGO was prepared by thermal exfoliation and reduction of GO.[46] The standard bars of HDPE/RGO nanocomposites of 50 mm × 4 mm × 2 mm in size with different RGO contents (0, 0.1, 0.5 and 1.0 wt%) were melt mixed using HAAKE MiniLab. The melt temperature, the screw speed, mold temperature and injection pressure were preset at 180 °C, 80 °C, 80 °C and 650 bar, respectively.

2.3. Analytical methods

Tensile test was performed on Instron 5567 at a tensile rate of 50 mm min^{-1}. Five standard bars for each sample were measured and the average values were calculated.

Differential scanning calorimetry (DSC) measurements were performed with Perkins Elmer DSC8000 under nitrogen atmosphere. All samples were first heated to 180 °C at a heating rate of 10 °C min^{-1}, and equilibrated at 180 °C for 5 min to remove thermal history. Subsequently, the samples were cooled to 30 °C at a cooling rate of 10 °C min^{-1}. The crystallinity of the HDPE in mass fraction, X_c, was calculated as follow:

$$X_c = \frac{\Delta H}{\Delta H_m^0} \times 100\% \quad (1)$$

where ΔH is the melting enthalpy of per gram of sample and ΔH_m^0 is the enthalpy of crystallization per gram of 100% crystalline HDPE, which is equal to 293 J g^{-1}.

2D WAXD experiments were carried out on the BL16B1 beam-line in the Shanghai Synchrotron Radiation Facility (SSRF). WAXD curves were collected from the 2D WAXD patterns. The wavelength of the monochromatic X-ray was 1.24 Å. The 2D diffraction patterns were recorded in transmission mode at room temperature.

2D SAXS experiments were carried out on the BL16B1 beam-line in the SSRF. The 2D patterns were recorded in transmission mode at room temperature and the sample-to-detector distance was 2000 mm.

The SAXS and WAXD data analysis were performed out by using the Fit2d software package.[47] The lamellae parameters derived from the SAXS data is named the long period L. It can be calculated according to the Bragg equation:

$$L = \frac{2\pi}{q^*} \quad (2)$$

q^* represents the peak position in the scattering curves.

3. Results and discussion

3.1. Mechanical properties

In order to investigate the influence of epitaxial crystallization on the mechanical properties of polymer matrix, tensile test was employed. Fig. 1 shows the stress–strain curves of pure HDPE and HDPE/RGO nanocomposites with different RGO contents and the inset shows the magnification around the yield point. It can be observed that the composite sample tends to reach the upper yield point with the increase of RGO contents. The effect

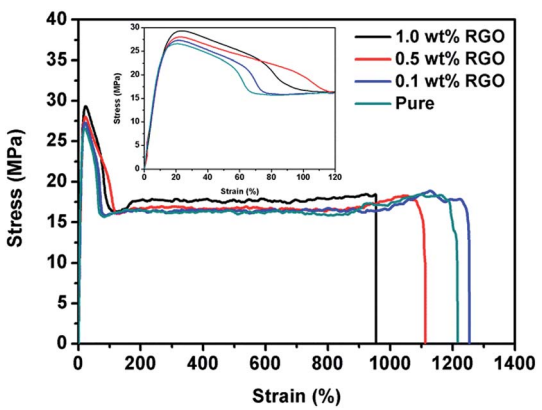

Fig. 1 Stress–strain curves of pure HDPE and its nanocomposites with various RGO contents.

of RGO content on the mechanical properties is shown in Fig. 2. Compared to pure HDPE, yield strength increases from 26.7 ± 0.3 to 29.6 ± 0.1 MPa and Young's modulus increases from 244.9 ± 6.1 to 379.4 ± 6.1 MPa for HDPE/RGO nanocomposites with 1.0 wt% RGO, which achieves 10.9 and 54.9% increase, respectively. This result is consistent with that of our previous work which showed the enhancement of PCL mechanical properties by RGO.[38]

3.2. Crystallization and orientation of HDPE/RGO nanocomposites

The DSC heating curves of neat iPP and iPP/RGO nanocomposites with different RGO loadings are shown in the Fig. 3a. The degree of crystallinity calculated from formula (1) is 62.5%, for pure HDPE, but the values increase to 56.1%, 57.0% and 58.4% as the RGO contents from 0.1 to 0.5, 1.0 wt%. These results are not agree with our previous work.[39] For the degree of crystallization decrease with 0.1 wt% RGO contents compare with the pure HDPE, we speculate that the incorporation of RGO destroys HDPE original lamellae and form smaller lamellae. While HDPE chains can be absorbed on the RGO surface and grow into crystals at the cooling process because of epitaxial crystallization. With the increase of RGO contents, the orientation degree of HDPE chains is enhanced. And the degree of crystallization of nanocomposite increases. The DSC cooling curves of pure HDPE and HDPE/RGO nanocomposites with different RGO contents are presented in Fig. 3b. The crystallization temperature (T_c) is around 110 °C for pure HDPE, while the T_c progressively shifts to high temperature with the increase of RGO contents from 0.1 wt% to 1.0 wt%. For example, it increases to 113 °C for HDPE/RGO-1.0 nanocomposites. These results indicate that RGO can significantly enhance the non-isothermal melt crystallization of HDPE.

3.3. WAXD analysis

The final properties of the injection molded bars are closely linked with the orientation of the lamellae in the nanocomposites. Fig. 4 gives the 2D WAXD patterns of injection-molded bars of pure HDPE and HDPE/RGO nanocomposites. From inner to outward, the diffraction circles are designated to the (110) and (200) crystal planes of polyethylene crystals, respectively. The corresponding WAXD curves of samples

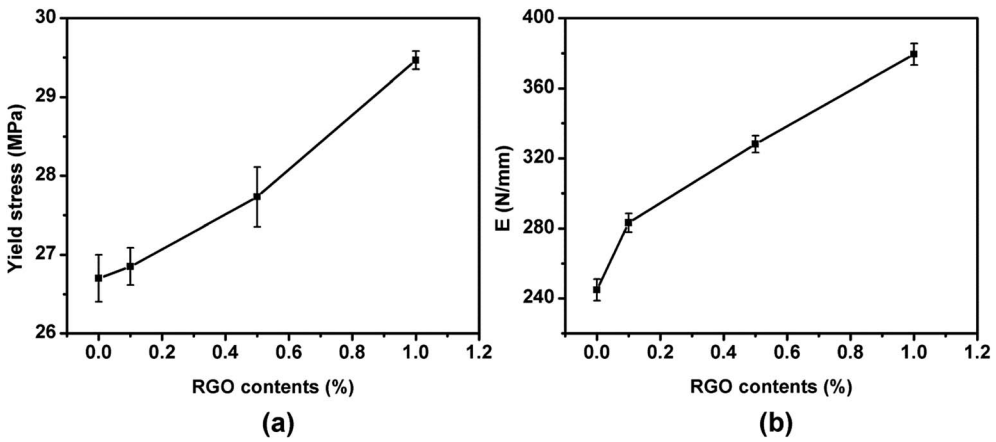

Fig. 2 The effect of RGO content on the mechanical properties: (a) yield stress (b) Young's modulus (*E*).

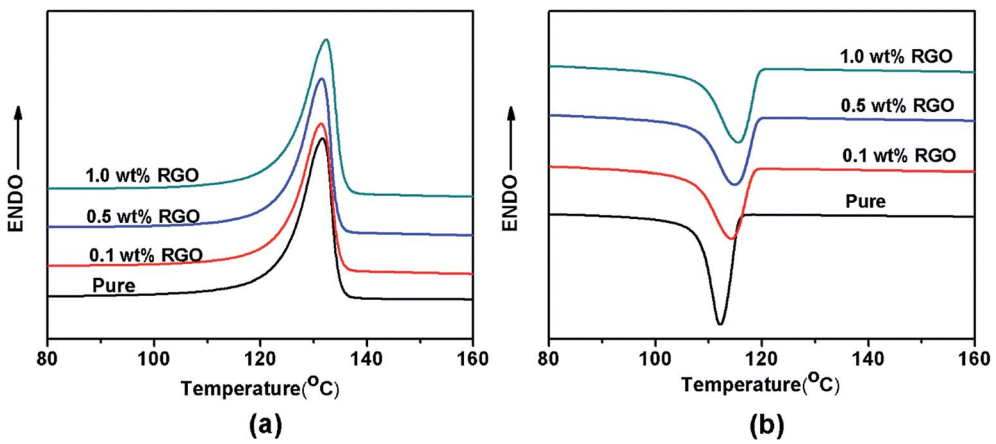

Fig. 3 Nonisothermal DSC scans of neat iPP and iPP/RGO nanocomposites with different RGO loadings (a) heating, (b) cooling.

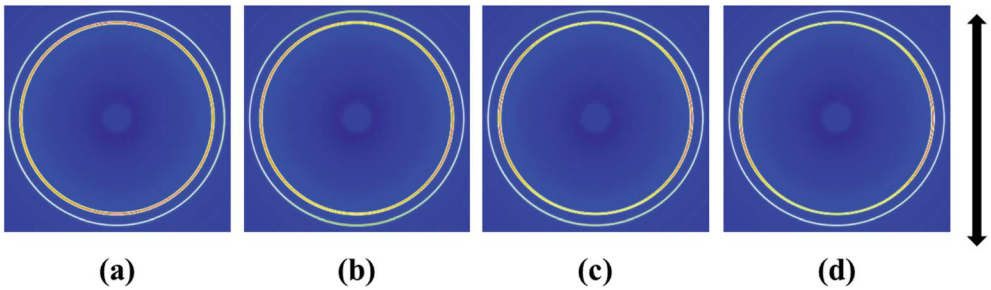

Fig. 4 2D WAXD patterns of pure HDPE (a) and its nanocomposites with different RGO contents: (b) 0.1 wt%, (c) 0.5 wt% and (d) 1.0 wt% (the arrow represents the orientation of the bars).

collected from 2D WAXD patterns show in Fig. 5, which present the same two typical diffraction peaks at $2\theta = 17.2^\circ$ and 19.2° corresponding to (110) and (200) crystal planes, respectively, suggesting that the crystal structure of HDPE remains unchanged despite the presence of RGO in the HDPE/RGO nanocomposites. It can be found in Fig. 4 that two isotropic circles are observed for pure HDPE, while two weakly focused diffraction focused arcs are found in the HDPE/RGO nanocomposites. The differences in the patterns demonstrate an enhancement of the crystalline orientation and an improvement of anisotropic degree of diffraction arcs with the increase of RGO content. It can be observed more clearly the influence of RGO on the crystallization of HDPE through 3D WAXD patterns shown in Fig. 6. With the increase of RGO content, the intensity of the two crystal plane diffraction rings are strengthened perpendicular to the sample injection flow direction and became less parallel to the injection flow direction. The differences in the 3D WAXD patterns indicate that the strong interaction between RGO and HDPE leads to more chain orientation and crystallization and the increase of RGO contents may hinders the relaxation of chains between HDPE and RGO during the orientation and crystallization process.

The 2D SAXS patterns from melt-crystallized isotropic samples typically display a strong scatting ring and one or two higher orders of much lower intensity. The SAXS pattern of an oriented sample typically displays strong two-point patterns with a maximum in the draw or flow direction or within certain angle about the reference direction.[48] Fig. 7 shows 2D SAXS patterns of pure HDPE and its nanocomposites. An almost isotropic reflection circle and two small scattering spots are observed in pure HDPE (Fig. 7a). For HDPE/RGO nanocomposites, small scattering spots gradually become bulb-shape lobes in the meridian direction with the increase of RGO. Moreover, the scattering disks change from circular ring for pure HDPE to elliptical ring for HDPE/RGO nanocomposites. It is different from our previous work that the PCL/RGO nanocomposites have no periodic structure in center part.[38] The result seems to indicate that more HDPE chains can epitaxial crystallize on the RGO surface than PCL. We can clearly observe the periodic structure at the center of the patterns for HDPE/RGO nanocomposites. The center of pure HDPE has no periodic structure, but with the increase of RGO contents, scattering pattern of direction in the equator and meridian direction the periodic structure are both enhanced. The changes of two parts of pure HDPE and its nanocomposites can be observed through 3D SAXS patterns (Fig. 8). Obviously, the scattering intensity of both ends is enhanced at the flow direction, at the same time the scattering intensity of the center is strengthened with the increase of RGO contents.

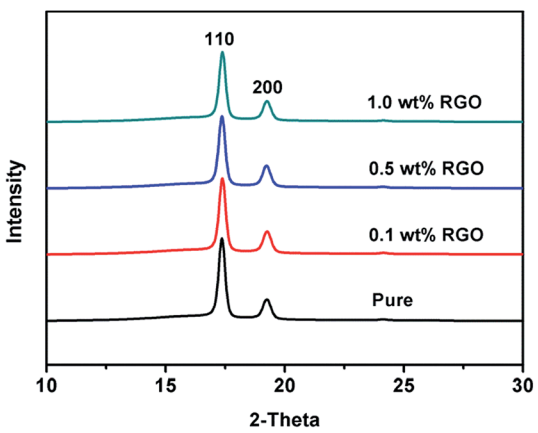

Fig. 5 WAXD curves of pure HDPE and HDPE/RGO nanocomposites with various RGO contents.

In order to investigate the orientation and periodic structure of HDPE matrix, SAXS intensity profiles of pure HDPE and its nanocomposites are further presented. Fig. 9a shows azimuthally integrated profiles of all samples. It can be observed that two weak peaks in pure HDPE parallel to the sample injection flow direction, which implies that the flow field can promote the orientation of HDPE crystals. The orientation degree of HDPE chains is enhanced significantly in the meridian direction and increased with the increase of RGO content. Fig. 9b shows the radially integrated profiles of meridian direction, the sharp peaks reflect the center part in the 2D SAXS patterns and the flat peaks reflect the scattering outer ring which are used to calculate the long period of HDPE matrix using the eqn (2). Apparently, for the two bulb-shape lobes all samples have the same long period calculated to be about 22.4 nm, suggesting regular aligned crystal lamellae in HDPE matrix. The q value of intensity valley (solid line in Fig. 9b) increases with the addition of RGO. These results indicate that the orientation of polymer chains is enhanced with the incorporation of RGO and the thickness of periodic structure increase.

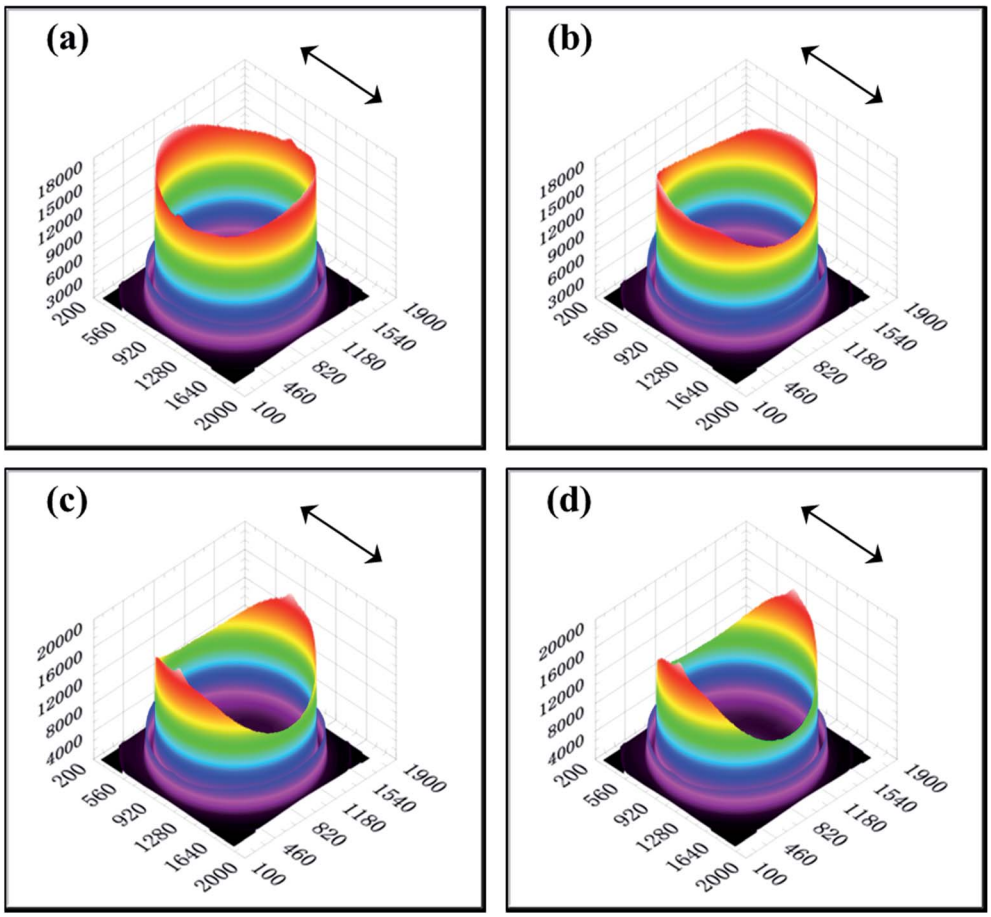

Fig. 6 3D WAXD patterns of pure HDPE (a) and its nanocomposites with different RGO contents: (b) 0.1 wt%, (c) 0.5 wt% and (d) 1.0 wt% (the arrows represent the orientation of the bars).

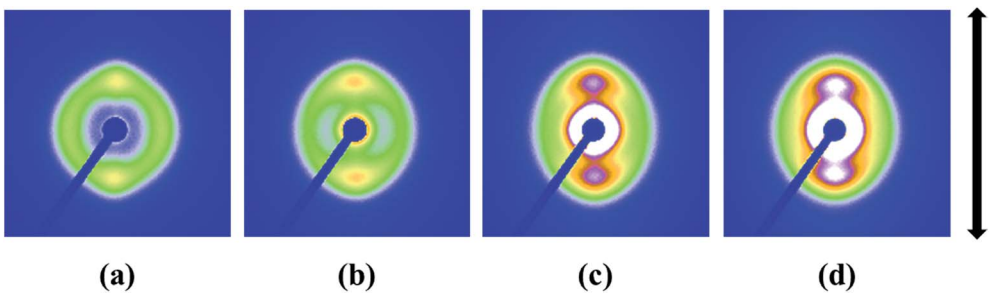

Fig. 7 2D SAXS patterns of pure HDPE (a) and its nanocomposites with different RGO contents: (b) 0.1 wt%, (c) 0.5 wt% and (d) 1.0 wt% (the arrow represents the orientation of the bars).

In our previous work, Wang *et al.* proved that RGO could induce PCL chain epitaxial crystallization on the surface, and the chains in the epitaxial crystallized lamellae were parallel to the flow direction in injection process.[38] On the basis of the aforementioned results in this paper, it can be concluded that the similar structural results are obtained in HDPE/RGO nanocomposites. Chen *et al.* reported that in the polymer/CNT composites, the CNT could preferentially orient parallel to the drawing direction in the stretched.[49,50] Similarly, the RGO sheets could orientation in thee flow direction, during injection process. The mechanism is thought to be similar to that of PCL/RGO nanocomposites in our previous work and it can be sketched as follows. Intensive shear flow during injection process not only leads 2D layered RGO sheets to the parallel orientation along flow direction but also stretches HDPE chains to high orientation even to extended form along same direction. Hu *et al.* proved that the relaxation of polymer chains would induce the loss in mechanical properties.[51] Paralleled 2D layered RGO sheets restrict the rapid mobility of HDPE chains resulting in delayed relaxation of oriented polymer chains.

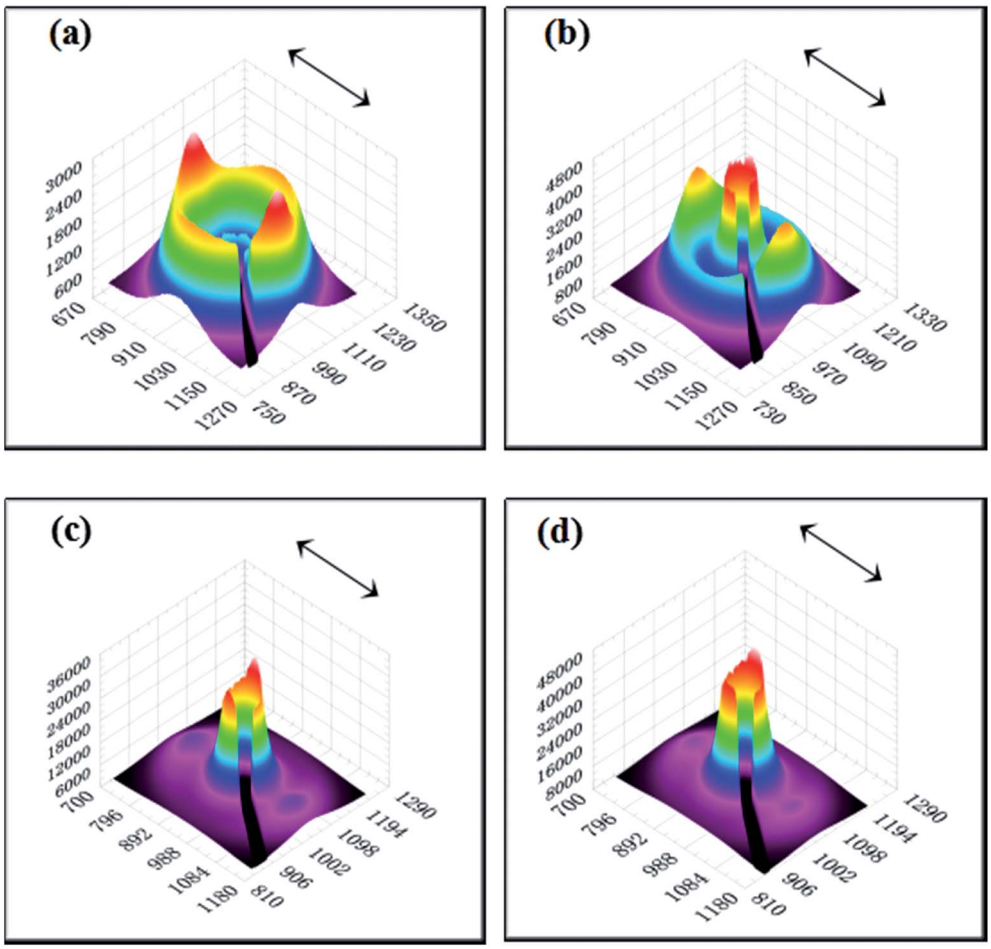

Fig. 8 3D SAXS patterns of pure HDPE (a) and its nanocomposites with different RGO contents: (b) 0.1 wt%, (c) 0.5 wt% and (d) 1.0 wt% (the arrows represent the orientation of the bars).

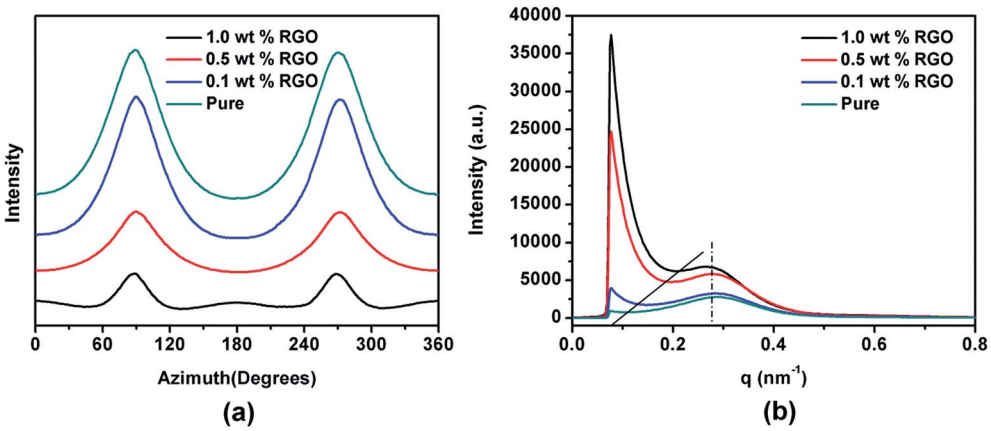

Fig. 9 Azimuthally integrated (a) and radially integrated, (b) profiles of pure HDPE and its nanocomposites with different RGO contents.

HDPE chains can be absorbed on the RGO surface and grow into crystals at the cooling process because of epitaxial crystallization. It is worth mentioning that the *c* axis is not completely paralleling to the flow direction on the basis of WAXD results above because the periodic structure of RGO is along three directions with the intersection angle of 60°. It should be noted that there seems more epitaxial crystallized crystals in HDPE/RGO nanocomposites compared to PCL/RGO nanocomposites from the SAXS result mentioned above. It is known that the epitaxial crystallization is due to the lattice matching between

RGO and polymer lamellae. Therefore the quantities of epitaxial crystallization on the surface of RGO during the injection process are generally determined by the lattice matching. The lattice mismatch R between an epitaxial crystal and a substrate crystal can be calculated as follows

$$R\,[\%] = \frac{d_E - d_S}{d_S} \times 100 \quad (3)$$

were d_E and d_S are spacings of 2D lattices at the interface of the epitaxial crystal and the substrate crystal, respectively. The a-axis of RGO was measured to be 0.246 nm.[52] Previous literature showed that the mismatch rate between polyethylene and graphene was −5.0%.[53] According to the crystal cell of PCL,[54] the mismatch rate between PCL and graphene was calculated to be $(1.726 - 0.246 \times 7)/(0.246 \times 7) = 0.2\%$. The epitaxial crystallization of HDPE on RGO is weaker than that of PCL only considering the mismatch rate. But it cannot be ignored that the calculation of mismatch rate between PCL and RGO above is based on seven periods and ester group in PCL chain seriously destroys the match between C–C and RGO. That more epitaxial crystallized crystals are obtained in HDPE/RGO nanocomposites may be attributed to the combination of the two above reasons. It is worth noting that the increase of mechanical properties of PCL/RGO nanocomposites is slightly higher than that of HDPE/RGO with same weight ratio RGO. It is may be due to that the affection of epitaxial crystallization on RGO on the mechanical properties of PCL is slightly higher because the mechanical properties are measured at room temperature which is near to the melting point of PCL compared to HDPE. According to the above analysis, the improvement in mechanical properties can be summed up in two aspects: one aspect is the natural excellent strength of graphene,[55] another one is speculated be attributed to epitaxial interaction between RGO and HDPE as the results exhibited above.

4. Conclusions

The effects of RGO on the crystallization and orientation of HDPE matrix in HDPE/RGO nanocomposites have been investigated by DSC, SAXS and WAXD measurements. The crystalline peak moves to the high temperature with the increase of RGO contents, indicating that RGO can significantly enhance the melt crystallization of HDPE. Though low orientation level of the matrix crystalline phase is observed in all nanocomposites but the WAXD results indicate that RGO can enhance the crystalline orientation of HDPE in the injection-molded bars. SAXS results suggest HDPE chains can be absorbed on the RGO surface and grow into crystals at the cooling process, which induces HDPE periodic structure increasing. This research is expected to be helpful for understanding the enhancement mechanism of layered nanofiller on the structures and corresponding mechanical properties of semi-crystalline polymer film or slice. To best understand the enhancement mechanism of polymer/layered nanofiller nanocomposites, especially for the nanofiller with space lattice matching to polymer, *in situ* structural evolution investigation during the stretching process of PCL/RGO and HDPE/RGO nanocomposites injection bars by online SAXS/WAXD measurements is ongoing.

Acknowledgements

This work was supported by the National Science Foundation of China (U1532114), Natural Science Foundation of Ningbo Municipal (2015A610021), and K. C. Wong Magna Fund in Ningbo University. Financially supported by the Opening Project of State Key Laboratory of Polymer Materials Engineering (Sichuan University) (Grant No. sklpme2016-4-26). We thank Shanghai Synchrotron Radiation Facility (SSRF) for supporting the SAXS and WAXD test.

References

1 P. B. Willis and C. H. Hsieh, *Kobunshi*, 2000, **49**, 52.
2 M. T. Demeuse, *Biaxial Stretching of Film: Principles and Applications*, Woodhead Publishing: Oxford, 2011.
3 J. S. Kang, T. H. Han, Y. J. Kang and H. Y. Chai, *Composites, Part B*, 2009, **40**, 404–412.
4 G. Choudalakis and A. D. Gotsis, *Eur. Polym. J.*, 2009, **45**, 967–984.
5 A. U. Chaudhry and V. Mittal, *Polym. Eng. Sci.*, 2013, **53**, 78–88.
6 Y. F. Chen, Y. Y. Qi, Z. X. Tai, X. B. Yan, F. L. Zhu and Q. J. Xue, *Eur. Polym. J.*, 2012, **48**, 1026–1033.
7 Z. Q. Hu and G. M. Chen, *Adv. Mater.*, 2014, **26**, 5950–5956.
8 L. R. Liang, C. Y. Gao, G. M. Chen and C. Y. Guo, *J. Mater. Chem. C*, 2016, **4**, 526–532.
9 M. Rahmat and P. Hubert, *Compos. Sci. Technol.*, 2011, **72**, 72–84.
10 B. Na, Q. Zhang, Q. Fu, G. Zhang and K. Z. Shen, *Polymer*, 2002, **43**, 7367–7376.
11 T. X. Liu, K. P. Lim, W. C. Tjiu, K. P. Pramoda and Z. K. Chen, *Polymer*, 2003, **44**, 3529–3535.
12 W. Cao, K. Wang, Q. Zhang, R. N. Du and Q. Fu, *Polymer*, 2006, **47**, 6857–6867.
13 P. Zhao, K. Wang, H. Yang, Q. Zhang, R. N. Du and Q. Fu, *Polymer*, 2007, **48**, 5688–5695.
14 K. Kalaitzidou, H. Fukushima and L. T. Drzal, *Composites, Part A*, 2007, **38**, 1675–1682.
15 K. Kalaitzidou, H. Fukushima and L. T. Drzal, *Carbon*, 2007, **45**, 1446–1452.
16 S. Kanagaraj, F. R. Varanda, T. V. Zhil'tsova, M. S. A. Oliveira and J. A. O. Simoes, *Compos. Sci. Technol.*, 2007, **67**, 3071–3077.
17 W. D. Zhang, L. Shen, I. Y. Phang and T. X. Liu, *Macromolecules*, 2004, **37**, 256–259.
18 I. Neitzel, V. Mochalin, I. Knoke, G. R. Palmese and Y. Gogotsi, *Compos. Sci. Technol.*, 2011, **71**, 710–716.
19 J. N. Coleman, U. Khan, W. J. Blau and Y. K. Gun'ko, *Carbon*, 2006, **44**, 1624–1652.
20 C. Peng, W. B. Hu, Y. T. Zhao, C. H. Fan and Q. Huang, *Small*, 2010, **6**, 1686–1692.
21 J. J. Ma, Y. Li, X. D. Yin, Y. Xu, J. Yue, J. J. Bao and T. Zhou, *RSC Adv.*, 2016, **6**, 49448–49458.

22 Z. J. Wang, F. Cheng, T. Winsor and Y. M. Liu, *Nanotechnology*, 2016, **27**, 412001.
23 K. L. Xu, G. M. Chen and D. Qiu, *J. Mater. Chem. A*, 2013, **1**, 12395–12399.
24 C. Y. Gao and G. M. Chen, *Compos. Sci. Technol.*, 2016, **124**, 52–70.
25 K. S. Novoselov, A. K. Geim, S. V. Morozov, D. Jiang, Y. Zhang, S. V. Dubonos, I. V. Grigorieva and A. A. Firsov, *Science*, 2004, **306**, 666–669.
26 C. Lee, X. Wei, J. W. Kysar and J. Hone, *Science*, 2008, **321**, 385–388.
27 H. Kim, A. A. Abdala and C. Macosko, *Macromolecules*, 2010, **43**, 6515–6530.
28 T. Kuilla, S. Bhadra, D. Yao, N. Kim, S. Bose and J. Lee, *Prog. Polym. Sci.*, 2010, **35**, 1350–1375.
29 R. Verdejo, M. M. Bernal, L. J. Romasanta and M. A. Lopez-Manchado, *J. Mater. Chem.*, 2011, **21**, 3301–3310.
30 E. Bekyarova, M. E. Itkis, P. Ramesh, C. Berger, M. Sprinkle, W. A. Herr and R. C. Haddon, *J. Am. Chem. Soc.*, 2009, **131**, 1336–1337.
31 Y. Li, *Polymer*, 2011, **52**, 2310–2318.
32 C. Shan, H. Yang, D. Han, Q. Zhang, A. Ivaska and L. Niu, *Langmuir*, 2009, **25**, 12030–12033.
33 J. T. Paci, T. Belytschko and G. C. Schatz, *Phys. Rev. B: Condens. Matter*, 2006, **74**, 184112.
34 J. Petermann, G. Broza, U. Rieck and A. Kawaguchi, *J. Mater. Sci.*, 1987, **22**, 1477–1481.
35 J. Petermann and Y. Xu, *Colloid Polym. Sci.*, 1991, **269**, 455–459.
36 B. Gross and J. Petermann, *J. Mater. Sci.*, 1984, **19**, 105–112.
37 T. Fukumaru, T. Fujigaya and N. Nakashima, *Macromolecules*, 2013, **46**, 4034–4253.
38 B. J. Wang, Y. J. Zhang, J. Y. Zhang, H. Y. Li, P. Chen, Z. B. Wang and Q. Gu, *Ind. Eng. Chem. Res.*, 2013, **52**, 15824–15828.
39 B. J. Wang, Y. G. Li, G. S. Weng, Z. Q. Jiang, P. Chen, Z. B. Wang and Q. Gu, *Compos. Sci. Technol.*, 2014, **96**, 63–70.
40 S. K. Yan, D. C. Yang and J. Petermann, *Polymer*, 1998, **39**, 4569–4578.
41 S. K. Yan, J. Petermann and D. C. Yang, *Polymer*, 1996, **37**, 2681–2685.
42 Y. J. Sun, H. H. Li, Y. Huang, E. Chen, L. Zhao, Z. H. Gan and S. K. Yan, *Polymer*, 2006, **47**, 2455–2459.
43 J. C. Wittmann and B. Lotz, *Prog. Polym. Sci.*, 1990, **15**, 909–948.
44 Y. Takenaka, H. Miyaji, A. Hoshino, A. Tracz, J. K. Jeszka and I. Kucinska, *Macromolecules*, 2004, **37**, 9667–9669.
45 Y. Wang, Z. H. Li, D. H. Hu, C. T. Lin, J. H. Li and Y. H. Lin, *J. Am. Chem. Soc.*, 2010, **132**, 9274–9276.
46 B. J. Wang, H. Y. Li, L. Z. Li, P. Chen, Z. B. Wang and Q. Gu, *Compos. Sci. Technol.*, 2013, **89**, 180–185.
47 A. P. Hammersley, S. O. Svensson and A. Thompson, *Nucl. Instrum. Methods Phys. Res.*, 1994, **346**, 312–321.
48 A. Prasad, R. Shrof, S. Rane and G. Beaucage, *Polymer*, 2001, **42**, 3103–3113.
49 C. P. Yuan, J. H. Zhang, G. M. Chen and J. P. Yang, *Chem. Commun.*, 2011, **47**, 899–901.
50 C. P. Yuan, J. J. Wang, G. M. Chen, J. H. Zhang and J. P. Yang, *Soft Matter*, 2011, **7**, 4039–4044.
51 W. B. Hu, A. Buzin, J. S. Lin and B. Wunderlich, *J. Polym. Sci., Part B: Polym. Phys.*, 2003, **41**, 403–417.
52 F. Tuinstra and E. Baer, *J. Polym. Sci., Part B: Polym. Phys.*, 1970, **8**, 861–865.
53 Y. Takenaka, H. Miyaji, A. Hoshino, A. Tracz, J. K. Jeszka and I. Kucinska, *Macromolecules*, 2004, **37**, 9667–9669.
54 H. L. Hu and D. L. Dorset, *Macromolecules*, 1990, **23**, 4604–4607.
55 C. G. Lee, X. D. Wei, J. W. Kysar and J. Hone, *Science*, 2008, **321**, 385–388.